
Calculation of Tropic Cyclone Inner Structure Using Quantum Theory with Ultimate Acceleration

Huaiyang Cui

Department of Physics, Beihang University, Beijing, 102206, China

Email: hycui@buaa.edu.cn

(September 26 2022 version 1, October 2 2023 version 2, submitted to viXra)

Abstract: In analogy with the ultimate speed c , there is an ultimate acceleration β , nobody's acceleration can exceed this limit β , in the solar system, $\beta=2.956391e+10(m/s^2)$. Because this ultimate acceleration is a large number, any effect related to β will become easy to test, including quantum gravity tests. In this paper, an approach is put forward to connect the ultimate acceleration with quantum theory, as an application, this approach is applied to tropic cyclone problems, the simulation is carried out, clearly showing the inner structure of a cyclone, which is very consistent with the famous DIANA cyclone on 12 September 1984 in situ observation measured by an aircraft.

1. Introduction

Some quantum gravity proposals [1,2] are extremely hard to test in practice, as quantum gravitational effects are appreciable only at the Planck scale [3]. But ultimate acceleration gives another scheme to deal with quantum gravity effects.

In analogy with the ultimate speed c , there is an ultimate acceleration β , nobody's acceleration can exceed this limit β , in the solar system, $\beta=2.956391e+10(m/s^2)$. Because this ultimate acceleration is a large number, any effect connecting to β will become easy to test, including quantum gravity tests.

In recent years, de Broglie matter wave has been generalized in terms of the ultimate acceleration, and is applied to the solar system to explain quantum gravity effects [28,29]. Consider a particle, its planetary-scale relativistic matter wave is given by the path integral

$$\psi = \exp\left(\frac{i\beta}{c^3} \int_0^x (u_1 dx_1 + u_2 dx_2 + u_3 dx_3 + u_4 dx_4)\right) . \quad (1)$$

where u is the 4-velocity of the particle, β is the ultimate acceleration determined by experiments. The β replaces the *Planck constant* in this quantum gravity theory so that *its wavelength becomes a length on planetary-scale*. This paper shows that the generalized matter wave can explain the solar quantum gravity effects correctly, and is successfully applied to the sunspot cycle and tropic cyclone problems.

2. Extracting ultimate acceleration from the solar system

In the orbital model as shown in Fig.1(a), the orbital circumference is n multiple of the wavelength of the planetary-scale relativistic matter wave, according to Eq. (1), consider a planet, we have

$$\left. \begin{aligned} \frac{\beta}{c^3} \oint_L v_l dl = 2\pi n \\ v_l = \sqrt{\frac{GM}{r}} \end{aligned} \right\} \Rightarrow \sqrt{r} = \frac{c^3}{\beta\sqrt{GM}} n; \quad n = 0, 1, 2, \dots \quad (2)$$

This orbital quantization rule only achieves a half success in the solar system, as shown in Fig.1(b), the Sun, Mercury, Venus, Earth and Mars satisfy the quantization equation; while other outer planets fail. But, since we only study quantum gravity effects among the Sun, Mercury, Venus, Earth and Mars, so this orbital quantization rule is good enough as a foundational quantum theory. In Fig.1(b), the blue straight line expresses a linear regression relation among the quantized orbits, so it gives $\beta=2.956391e+10$ (m/s²) by fitting the line. The quantum numbers $n=3,4,5,\dots$ were assigned to the solar planets, the sun was assigned a quantum number $n=0$ because the sun is in the **central state**.

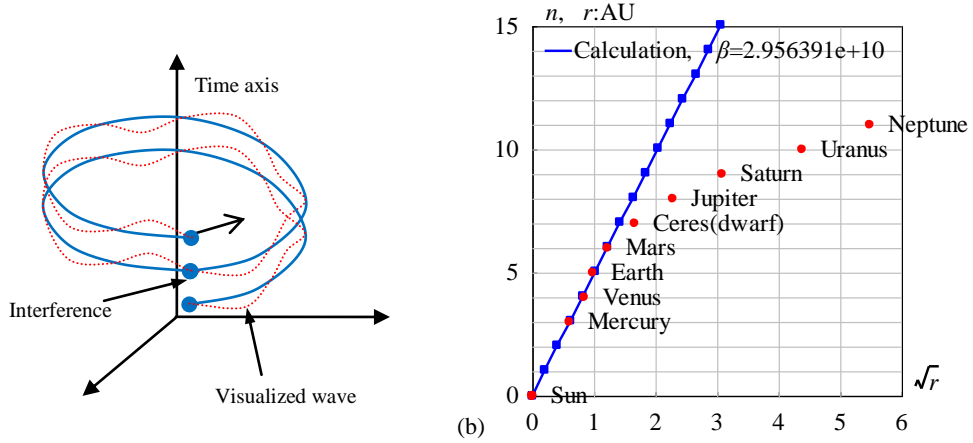


Fig.1 (a)The head of the relativistic matter wave may overlap with its tail. (b) The inner planets are quantized.

In the solar interior, if the coherent length of the relativistic matter wave is long enough, its head may overlap with its tail when the particle moves in a closed orbit, as shown in Fig.1(a). Consider a point on the solar equatorial plane, the overlapped wave is given by

$$\begin{aligned} \psi &= \psi(r)T(t) \\ \psi(r) &= 1 + e^{i\delta} + e^{i2\delta} + \dots + e^{i(N-1)\delta} = \frac{1 - \exp(iN\delta)}{1 - \exp(i\delta)} \quad (3) \end{aligned}$$

$$\delta(r) = \frac{\beta}{c^3} \oint_L (v_l) dl = \frac{2\pi\beta\omega r^2}{c^3}$$

where N is the overlapping number which is determined by the coherent length of the relativistic matter wave, δ is the phase difference after one orbital motion, ω is the angular speed of the solar self-rotation. The above equation is a multi-slit interference formula in optics, for a larger N it is called as the Fabry-Perot interference formula.

The planetary-scale relativistic matter wave function ψ needs a further explanation. In quantum mechanics, $|\psi|^2$ equals to the probability of finding an electron due to Max Born's explanation; in astrophysics, $|\psi|^2$ equals to the probability of finding a nucleon (proton or neutron) *averagely on an astronomic scale*, we have

$$|\psi|^2 \propto \text{nucleon-density} \propto \rho . \quad (4)$$

It follows from the multi-slit interference formula that the overlapping number N is estimated by

$$N^2 = \frac{|\psi(0)_{\text{multi-wavelet}}|^2}{|\psi(0)_{\text{one-wavelet}}|^2} = \frac{\rho_{\text{core}}}{\rho_{\text{surface_gas}}} . \quad (5)$$

The solar core has a mean density of 1408 (kg/m³), the surface of the sun is comprised of convective zone with a mean density of 2e-3 (kg/m³) [7]. In this paper, the sun's radius is chosen at a location where density is 4e-3 (kg/m³), thus the solar overlapping number N is calculated to be $N=593$. Since the mass density $\rho(r)$ has spherical symmetry, then the $\psi(r)$ has the spherical symmetry.

Sun's angular speed at its equator is known as $\omega=2\pi/(25.05 \times 24 \times 3600)$ (s⁻¹). Its mass 1.9891e+30 (kg), well-known radius 6.95e+8 (m), mean density 1408 (kg/m³), the constant $\beta=2.956391 \times 10^{10}$ (m/s²). According to the $N=593$, the matter distribution of the $|\psi|^2$ is calculated in Fig.2(a), it agrees well with the general description of star's interior. The radius of the sun is determined as $r=7 \times 10^8$ (m) with a relative error of 0.72% in Fig.2, which indicates that the sun radius strongly depends on the sun's self-rotation.

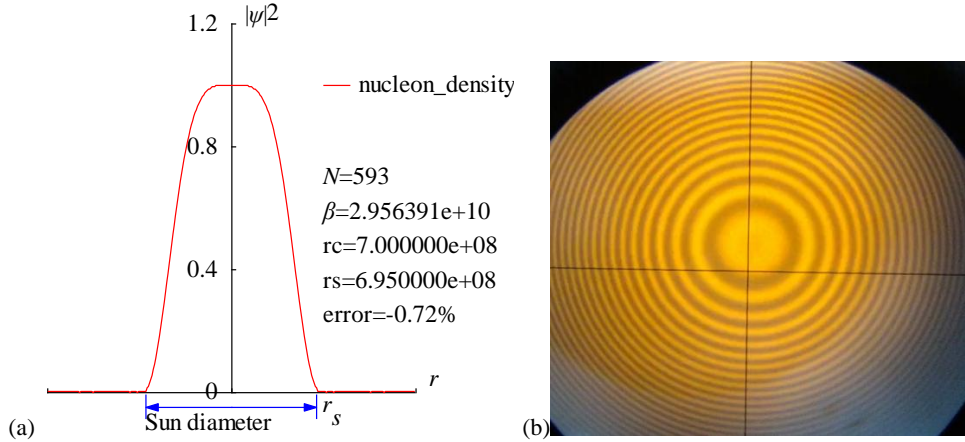


Fig.2 (a)The nucleon distribution $|\psi|^2$ in the Sun is calculated in the radius direction. (b) As contrast, sodium Fabry-Perot interference ($\delta=\text{const.}$).

```
<Clet2020 Script>/C source code [26]
int i,j,k,m,n,N,nP[10];
double beta,H,B,M,r,r_unit,x,y,z,delta,D[1000],S[1000], a,b,rs,rc,omega,atm_height; char str[100];
main(){k=150;rs=6.95e8;rc=0;x=25.05;omega=2*PI/(x*24*3600);n=0; a=1408/0.004; N=sqrt(a);
beta=2.956391e10;H=SPEEDC*SPEEDC*SPEEDC/beta;M=1.9891E30; atm_height=2e6; r_unit=1E7;
for(i=-k;i<k;i+=1) {r=abs(i)*r_unit;
if(r<rs+atm_height) delta=2*PI*omega*r*r/H; else delta=2*PI*sqrt(GRAVITYC*M*r)/H;//around the star
x=1;y=0; for(j=1;j<N;j+=1) { z=delta*j; x+=cos(z);y+=sin(z);} z=x*x+y*y; z=z/(N*N);
S[n]=i;S[n+1]=z; if(i>0 && rc==0 && z<0.0001) rc=r; n+=2;}
SetAxis(X_AXIS,-k,0,k,"#ifr; ;");SetAxis(Y_AXIS,0,0,1.2,"#if|psi|su2#;0;0.4;0.8;1.2;");
DrawFrame(FRAME_SCALE,1,0xaffaf); z=100*(rs-rc)/rs;
SetPen(1,0xff0000);Polyline(k+k,S,k/2,1," nucleon_density"); SetPen(1,0x0000ff);
r=rs/r_unit;y=-0.05;D[0]=-r;D[1]=y;D[2]=r;D[3]=y; Draw("ARROW,3,2,XY,10,100,10,10,"D);
Format(str,"#ifN#t=%d#n#i#f#t=%e#nrc=%e#nrs=%e#nerror=%.2f%",N,beta,rc,rs,z);
TextHang(k/2,0.7,0,str);TextHang(r+5,y/2,0,"#ifr#sds#");TextHang(-r,y+y,0,"Sun diameter");
}#v07=?>A
```

3. Extracting ultimate acceleration from the earth

Applying the planetary-scale relativistic matter wave to the Moon, as illustrated in Fig.3, The moon is assigned a quantum number of $n=2$ because some quasi-satellite's perigees have reached a depth almost at $n=1$ orbit, as shown in Fig.3. Here, the ultimate acceleration $\beta=1.377075e+14(m/s^2)$ is determined uniquely by the line between the earth and moon in Fig.3 by Eq. (2).

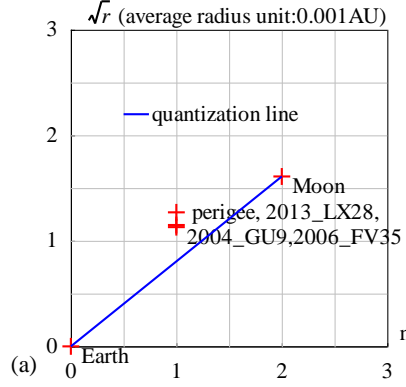


Fig.3 Orbital quantization for the moon.

```

<Clet2020 Script>// C source code [26]
char str[200];int i,j,k,N,nP[10]; double x,y,z,M,r_unit,a,b,B,H,r_ave[20],dP[10],D[1000];
double orbit[10]={0.2,57.0,}; double e[10]={0, 0.0549,0,0,0,0,0,0,0,};
int qn[10]={0.2,3,4,5,6,7,8,9,10,};
char Stars[100]={"Earth;Moon;"};
int main(){ N=2; M=5.97237E24; r_unit=1.495978707e8;
for(i=0;i<N;i+=1) {x=orbit[i];y=e[i]; z=x*(1+sqrt(1-y*y))/2;r_ave[i]=z;//average_radius
D[i+1]=qn[i];D[i+i+1]=sqrt(z); }
DataJob("REGRESSION,2",D,dP);b=dP[0];a=dP[1];
SetAxis(X_AXIS,0,0,3,"n:0;1;2;3;");
SetAxis(Y_AXIS,0,0,3,"#i#r#t#t (average radius unit:0.001AU);0;1;2;3;");
DrawFrame(0x0166,1,0xaffaf); Polyline(N,D);
SetPen(2,0xff0000); Plot("OVALFILL,0,2,XY,3,3,"D);
for(i=0;i<N;i+=1) {nP[0]=TAKE;nP[1]=i;TextJob(nP,Stars,str);x=qn[i]+0.2;y=sqrt(orbit[i])-0.05;TextHang(x,y,0,str);}
x=GRAVITYC*M*r_unit; z=sqrt(x); H=z*a; B=-z*b;
TextAt(100,450,"#i#r#t=%e #i#B#t=%e",H,B);
for(i=0;i<N;i+=1) {y=b+a*qn[i];D[i+1]=qn[i];D[i+i+1]=y;}
SetPen(1,0x0000ff);Polyline(N,D,0.5,2.2,"quantization");//check
}#v07=?>A

```

Now let us talk about the earth's interior, the earth has a mean density of $5530 (kg/m^3)$, its surface is covered with air and vapor with a density of $1.29 (kg/m^3)$. The earth's radius is chosen at the sea level, it follows Eq.(5) that the earth's overlapping number N is calculated to be $N=65$.

The earth's angular speed is known as $\omega=2\pi/(24 \times 3600) (s^{-1})$, its mass $5.97237e+24 (kg)$, the well-known radius is $6.378e+6 (m)$, the earth's constant $\beta=1.377075e+14 (m/s^2)$. The matter distribution $|\psi|^2$ in radius direction is calculated by Eq.(3), as shown in Fig.4(a). The radius of the earth is determined as $r=6.4328e+6 (m)$ with a relative error of 0.86%, it agrees well with common knowledge. Space debris over the atmosphere has a complicated evolution [7,8], has itself speed

$$v_l = \sqrt{\frac{GM}{r}}; \quad \delta(r) = \frac{\beta}{c^3} \oint_L (v_l) dl = \frac{2\pi\beta}{c^3} \sqrt{GM} r \cdot \quad (6)$$

The secondary peaks over the atmosphere up to 2000km altitude are calculated out in Fig.4(b) which agrees well with the space debris observations [16]; the peak near 890 km altitude is due

principally to the January 2007 intentional destruction of the Fengyun-1C weather spacecraft, while the peak centered at approximately 770 km altitude was created by the February 2009 accidental collision of Iridium 33 (active) and Cosmos 2251 (derelict) communication spacecraft [16,18]. The observations based on the incoherent scattering radar EISCAT ESR located at 78°N in Jul. 2006 and in Oct. 2015 [21,22,23] are respectively shown in Fig.4(c) and (d). This prediction to secondary peaks also agrees well with other space debris observations [24,25].

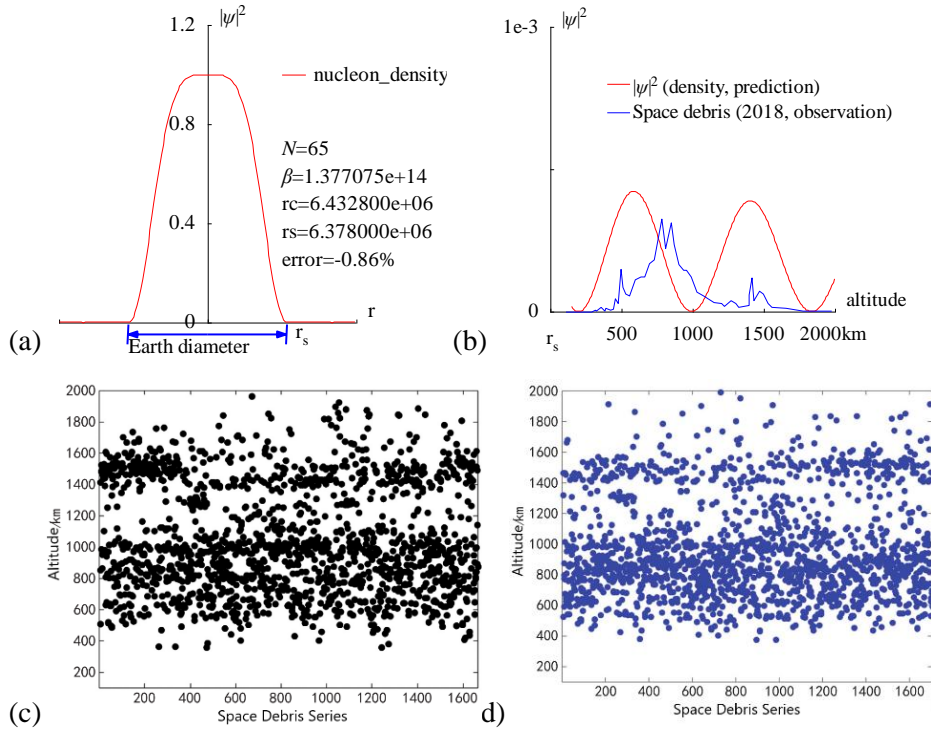


Fig.4 (a) The radius of the Earth is calculated out $r=6.4328e+6$ (m) with a relative error 0.86% by the interference of its acceleration-roll wave; (b) The prediction of the space debris distribution up to 2000km altitude; (c) The space debris distribution in Jul. 2006, Joint observation based on the incoherent scattering radar EISCAT ESR located at 78°N [21]; (d) The space debris distribution in Oct. 2015, Joint observation based on the incoherent scattering radar EISCAT ESR located at 78°N [21].

```
<Clet2020 Script>//C source code [26]
int i,j,k,m,n,N,nP[10]; double H,B,M,v_r,r,AU,r_unit,x,y,z,delta,D[10],S[1000];
double rs,rc,rot,a,b,atm_height,beta; char str[100];
main(){k=80;rs=6.378e6;rc=0;atm_height=1.5e5;n=0;N=65;
beta=1.377075e+14;H=SPEEDC*SPEEDC*SPEEDC/beta;
M=5.97237e24;AU=1.496E11;r_unit=1e-6*AU; rot=2*PI/(24*60*60);//angular speed of the Earth
for(i=-k;i<k;i+=1){r=abs(i)*r_unit;
if(r<rs+atm_height)v_r=rot*r; else v_r=sqrt(GRAVITYC*M/r);//around the Earth
delta=2*PI*v_r/H; y=SumJob("SLIT_ADD,@N,@delta",D); y=y/(N*N);
if(y>1)y=1; S[n]=i;S[n+1]=y; if(i>0 && rc==0 && y<0.001)rc=r; n+=2;}
SetAxis(X_AXIS,-k,0,k,"r"; ; );SetAxis(Y_AXIS,0,0,1.2,"#i|ψ|²#su2#t;0;0.4;0.8;1.2;");
DrawFrame(FRAME_SCALE,1,0,0,0,0); x=50;z=100*(rs-rc)/rs;
SetPen(1,0,0,0,0);Polyline(k+k,S,k/2,1," nucleon_density");
r=rs/r_unit;y=-0.05;D[0]=-r;D[1]=y;D[2]=r;D[3]=y;
SetPen(2,0,0,0,0); Draw("ARROW,3,2,XY,10,100,10,10," ,D);
Format(str,"#iN#t=%d#n#iβ#t=%e#nrc=%e#nrs=%e#nerror=%.2f%",N,beta,rc,rs,z);
TextHang(k/2,0.7,0,str);TextHang(r+5,y/2,0,"r#sds#t");TextHang(-r,y+y,0,"Earth diameter");
}#v07=?>A#t
<Clet2020 Script>//C source code [9]
int i,j,k,m,n,N,nP[10]; double H,B,M,v_r,r,AU,r_unit,x,y,z,delta,D[10],S[10000];
double rs,rc,rot,a,b,atm_height,p,T,R1,R2,R3; char str[100]; int
Debris[96]={110,0,237,0,287,0,317,2,320,1,357,5,380,1,387,4,420,2,440,3,454,14,474,9,497,45,507,26,527,19,557,17,597,34,63
4,37,664,37,697,51,727,55,781,98,808,67,851,94,871,71,901,50,938,44,958,44,991,37,1028,21,1078,17,1148,10,1202,9,1225,6,
1268,12,1302,9,1325,5,1395,7,1395,18,1415,36,1429,12,1469,22,1499,19,1529,9,1559,5,1656,4,1779,1,1976,1,};
main(){k=80;rs=6.378e6;rc=0;atm_height=1.5e5;n=0;N=65;
H=1.956611e11;M=5.97237e24;AU=1.496E11;r_unit=1e4;
rot=2*PI/(24*60*60);//angular speed of the Earth
b=PI/(2*PI*rot*rs/H); R1=rs/r_unit;R2=(rs+atm_height)/r_unit;R3=(rs+2e6)/r_unit;
```

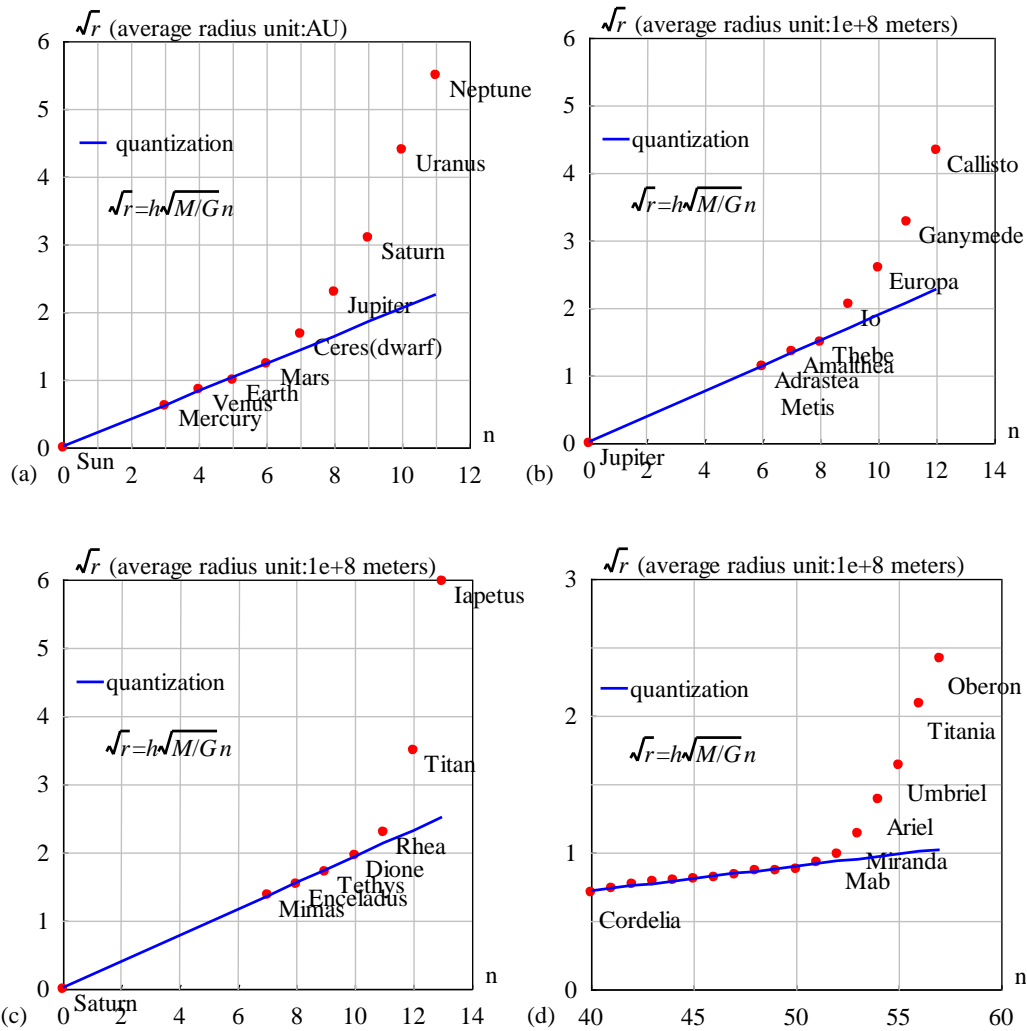
```

for(i=R2;i<R3;i+=1) {r=abs(i)*r_unit; delta=2*PI*sqrt(GRAVITYC*M*r)/H;
y=SumJob("SLIT_ADD,@N,@delta",D); y=1e3*y/(N*N);// visualization scale:1000
if(y>1) y=1; S[n]=i;S[n+1]=y;n+=2;}
SetAxis(X_AXIS,R1,R1,R3,"altitude; r#sds#t;500;1000;1500;2000km ;");
SetAxis(Y_AXIS,0,0,1,"#if#w/#su2#t;0; ;1e-3;");DrawFrame(FRAME_SCALE,1,0,affaf); x=R1+(R3-R1)/5;
SetPen(1,0,ff0000);Polyline(n/2,S,x,0.8,"#if#w/#su2#t (density, prediction)");
for(i=0;i<48;i+=1) {S[i+i]=R1+(R3-R1)*Debris[i+i]/2000; S[i+i+1]=Debris[i+i+1]/300;}
SetPen(1,0,0000ff);Polyline(48,S,x,0.7,"Space debris (2018, observation) "); }#v07=?>A#t

```

4. Planck-Constant-like Constant

The solar system, Jupiter's satellites, Saturn's satellites, Uranus' satellites, and Neptune's satellites as five different many-body systems are investigated with the Bohr's orbit model. After fitting observational data as shown in Fig.5, their ultimate accelerations are obtained and listed in Table 1. The predicted quantization blue-lines in Fig.5(a), Fig.5(b), Fig.5(c), Fig.5(d) and Fig.5(e) agree well with experimental observations for those *inner constituent planets or satellites*.



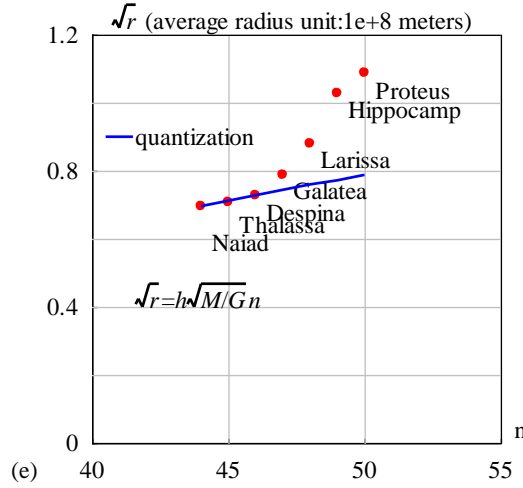


Fig.5 The orbital radii are quantized for inner constituents. (a) the solar system with $h=4.574635e-16$ ($m^2s^{-1}kg^{-1}$). The relative error is less than 3.9%. (b) the Jupiter system with $h=3.531903e-16$ ($m^2s^{-1}kg^{-1}$). Metis and Adrastea are assigned the same quantum number for their almost same radius. The relative error is less than 1.9%. (c) the Saturn system with $h=6.610920e-16$ ($m^2s^{-1}kg^{-1}$). The relative error is less than 1.1%. (d) the Uranus system with $h=1.567124e-16$ ($m^2s^{-1}kg^{-1}$). $n=0$ is assigned to Uranus. The relative error is less than 2.5%. (e) the Neptune system with $h=1.277170e-16$ ($m^2s^{-1}kg^{-1}$). $n=0$ is assigned to Neptune. The relative error is less than 0.17%.

Table 1 Planck-constant-like constant h , N is constituent particle number with smaller inclination.

system	N	M/M_{earth}	β (m/s^2)	h ($m^2s^{-1}kg^{-1}$)	Prediction
Solar planets	9	333000	2.961520e+10	4.574635e-16	Fig.5(a)
Jupiter' satellites	7	318	4.016793e+13	3.531903e-16	Fig.5(b)
Saturn's satellites	7	95	7.183397e+13	6.610920e-16	Fig.5(c)
Uranus' satellites	18	14.5	1.985382e+15	1.567124e-16	Fig.5(d)
Neptune 's satellites	7	17	2.077868e+15	1.277170e-16	Fig.5(e)

Besides every β , our interest shifts to the constant h in Table 1, which is defined as

$$h = \frac{c^3}{M\beta} \quad (7)$$

In a many-body system with a total mass of M , the wavelength of the planetary-scale relativistic matter for a moving particle with the speed v becomes

$$\lambda = \frac{2\pi h M}{v}; \quad \psi = \exp\left(\frac{i}{hM} \int_0^x (u_1 dx_1 + u_2 dx_2 + u_3 dx_3 + u_4 dx_4)\right) \quad (8)$$

where h is a **Planck-constant-like constant**. Usually, the total mass M is approximately equal to the central-star's mass. It is found that this generalized matter wave works correctly for quantizing orbits for inner constituents in Fig.5. The key point is that the various systems have almost the same Planck-constant-like constant h in Table 1 with a mean value of $3.51e-16$ $m^2s^{-1}kg^{-1}$, at least having the same order of magnitude!

5. First example of gravity-clock: Sunspot cycle

The **coherence length** of waves is usually mentioned but the **coherence width** of waves is rarely discussed in quantum mechanics, simply because the latter is not a matter for electrons, nucleon, or photons, but it is a matter in astrophysics. The analysis of observation data tells us that on the planetary scale, the coherence width of planetary-scale relativistic matter waves can extend to 1000 kilometers or more, as illustrated in Fig.6(a), the overlap may even occur in the orbital width direction, thereby bringing new aspects to wave interference.

In the solar convective zone, adjacent convective rings form a top-layer flow, a middle-layer gas, and a ground-layer flow. Considering one convective ring at the equator as shown in Fig.6(b), there is an apparent velocity difference between the top-layer flow and the middle-layer gas, where their planetary-scale relativistic matter waves are denoted respectively by

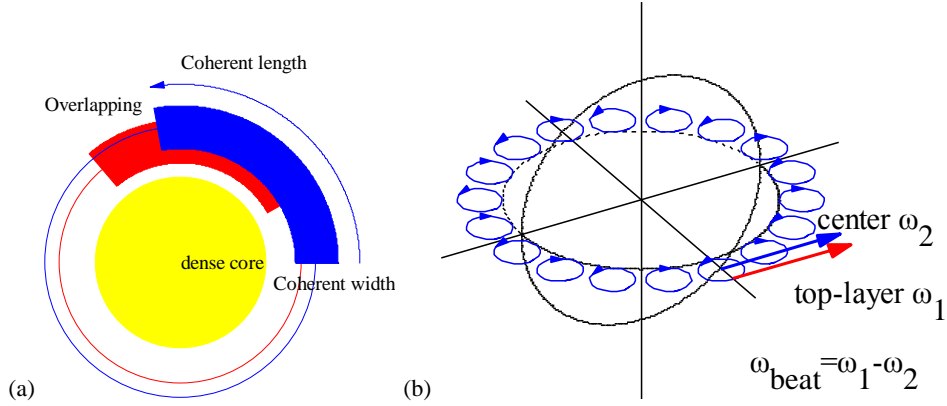


Fig.6 (a) Illustration of overlapping in the coherent width direction. (b) Convective rings at the equator.

$$\begin{aligned}\psi_{top} &= \exp\left[\frac{i\beta}{c^3} \int_L (v_1 dl + \frac{-c^2}{\sqrt{1-v_1^2/c^2}} dt)\right] \\ \psi_{middle} &= \exp\left[\frac{i\beta}{c^3} \int_L (v_2 dl + \frac{-c^2}{\sqrt{1-v_2^2/c^2}} dt)\right]\end{aligned}\quad (9)$$

Their interference in the coherent width direction leads to a beat phenomenon

$$\begin{aligned}|\psi|^2 &= |\psi_{top} + C\psi_{middle}|^2 = 1 + C^2 + 2C \cos\left[\frac{2\pi}{\lambda_{beat}} \int_L dl - \frac{2\pi}{T_{beat}} t\right] \\ \frac{2\pi}{T_{beat}} &= \frac{\beta}{c^3} \left(\frac{c^2}{\sqrt{1-v_1^2/c^2}} - \frac{c^2}{\sqrt{1-v_2^2/c^2}} \right) \approx \frac{\beta}{c^3} \left(\frac{v_1^2}{2} - \frac{v_2^2}{2} \right) \\ \frac{2\pi}{\lambda_{beat}} &= \frac{\beta}{c^3} (v_1 - v_2)\end{aligned}\quad (10)$$

where C is the coupling coefficient, their speeds are calculated as

$$\begin{aligned}v_1 &\approx 6100 \text{ (m/s)} \quad (\approx \text{observed in Evershed flow}) \\ v_2 &= \omega r_{middle} = 2017 \text{ (m/s)} \quad (\text{solar rotation});\end{aligned}\quad (11)$$

Where, regarding the Evershed flow as the eruption of the top-layer flow, about 6 (km/s) speed was reported [31]. Alternatively, the top-layer speed v_1 also can be calculated in terms of

thermodynamics, to be $v_1=6244$ (m/s) [28]. Here using $v_1=6100$ (m/s), their beat period T_{beat} is calculated to be a value of 10.95 (years), in agreement with the sunspot cycle value (say, mean 11 years).

$$T_{beat} \approx \frac{4\pi c^3}{\beta(v_1^2 - v_2^2)} = 10.95 \text{ (years)} . \quad (12)$$

```
<Clet2020 Script>// C source code [26]
double beta,H,M,N,dP[20],D[2000],r,rs,rot,x,y,v1,v2,K1,K2,T1,T2,T,Lamda,V; int i,j,k,s;
int main(){beta=2.956391e10; H=SPEEDC*SPEEDC*SPEEDC/beta;
M=1.9891E30; rs=6.95e8;rot=2*PI/(25.05*24*3600);v1=rot*rs;K1=v1*v1/2;//T1=2*PI*H/K1;
v2=6100; K2=v2*v2/2;T2=2*PI*H/(K2-K1);T=T2/24*3600*365.2422;
Lamda=2*PI*H/(v2-v1);V=Lamda/T2;s=1;
SetViewAngle("temp0,theta60,phi-60");
DrawFrame(FRAME_LINE,1,0xaffaf);Overlook("2,1,60",D);
TextAt(10,10,"v1=%d, v2=%d, T=%.2f y, λ=%e, V=%d",v1,v2,T,Lamda,V);
SetPen(1,0x4f4fff); for(i=0;i<18;i+=1) {v1=i*2*PI/18; x=70*cos(v1);y=70*sin(v1);Ring();}
SetPen(2,0xff0000);Draw("ARROW,0,2,XYZ,15", "80,0,0,80,60,0");
TextHang(100,20,0,"top-layer ω#sd1#t"); SetPen(2,0x0000ff);
Draw("ARROW,0,2,XYZ,15", "70,0,0,70,60,0");
TextHang(50,60,0,"center ω#sd2#t");TextHang(140,-30,0," ω#sbeat#t=ω#sd1#t-ω#sd2#t");
}
Ring(){ k=0;N=20; r=10;
for(j=0;j<N+2;j+=1) {k=j+j+j; v2=s*j*2*PI/N; D[k]=x+r*cos(v2);D[k+1]=y+r*sin(v2); D[k+2]=0;}
Plot("POLYLINE,4,22,XYZ,8",D)s*=-1;}
#v07=?>A
```

The relative error to the mean 11 years is 0.6% for the beat period calculation using the planetary-scale relativistic matter waves. This beat phenomenon turns out to be a **nucleon density oscillation** that undergoes to drive the sunspot cycle evolution with a **gravity-clock**. The beat wavelength λ_{beat} is too long to observe, only the beat period (gravity-clock) is easy to be observed.

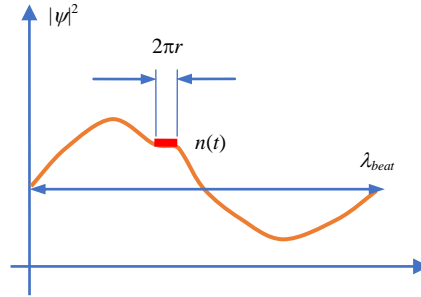


Fig.7 The equatorial circumference $2\pi r$ only occupies a little part of the beat wavelength, what we see is the expansion and contraction of the nucleon density.

As illustrated in Fig.7, on the solar surface, the equatorial circumference $2\pi r$ only occupies a little part of the beat wavelength, what we see is the expansion and contraction of the nucleon density.

$$\frac{2\pi r}{\lambda_{beat}} = 0.0031 . \quad (13)$$

This nucleon density oscillation is understood as a new type of nuclear reaction on an astronomic scale.

6. Second example of gravity-clock: Season clock

Consider a planetary-scale relativistic matter wave ψ_A in the earth shell at the latitude angle A , it will interfere with its neighbor waves within its coherent width. Because the earth shell mainly consists of dense matter, their mutual cascade-interference will cause the relativistic matter waves to have spherical symmetry, so that the relativistic matter wave ψ_A at the latitude angle A should equal to the $\psi_{equator}$ at the equator, as shown in Fig.8(a). This property is supported by the spherical symmetry of the earth's density distribution:

$$\begin{aligned} \text{spherical symmetry: } \rho(r, A, \varphi) = \rho(r) &\Rightarrow \psi(r, A, \varphi) = \psi(r) \\ \text{or: } \psi_A = \psi_{equator} \end{aligned} \quad (14)$$

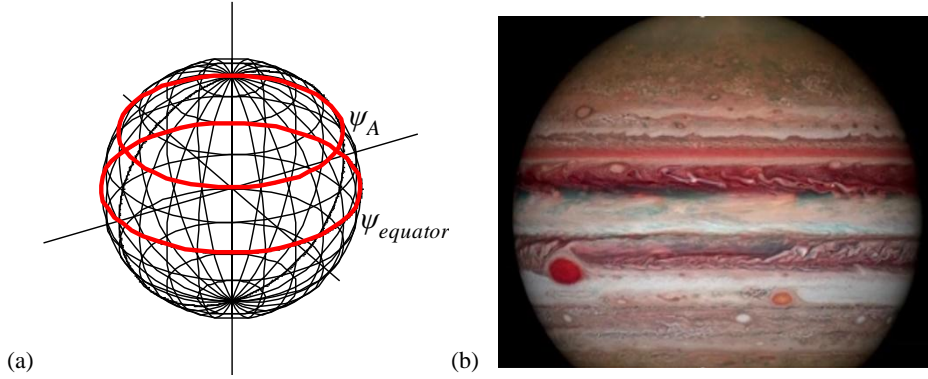


Fig.8 (a) Mutual cascade-interference will lead to the symmetry of the earth's density distribution. (b) Zonal winds on Jupiter (the photo from public News).

On the contrary, in the thin atmosphere, the wind and clouds are freely distributed in the sky on a large scale, because their cascade-interference within coherence width can be ignored.

Using the coherent width concept, considering the interference between the air ψ_A at the latitude angle A and the shell ψ_{shell} at the same latitude, their interference is given by

$$\begin{aligned} \psi(r, A) = \psi_{air}(r, A) + C\psi_{shell}(r, A) &= \psi_{air}(r, A) + C\psi_{shell_equator}(r) \\ T_{beat} &\approx \frac{4\pi c^3}{\beta(v_{shell_equator}^2 - v_{air}^2)} \end{aligned} \quad (15)$$

$$v_{shell_equator} = \omega r$$

$$v_{air} = \omega r \cos(A) + v_{wind} + v_{sun_effect}$$

where C represents the coupling constant which relates to their distance and their mass fractions, their interference leads to a beat phenomenon. Positive wind defined as in the direction from west to east, the term v_{sun_effect} represents the action of the sun on the air. The beat phenomenon is characterized as follows.

(1) Forced Oscillation

Due to the tilt of 23.5° of the earth axis with respect to the earth's orbital plane, the directly shined latitude A_1 sways within $A=23.5^\circ \text{ S} \sim 23.5^\circ \text{ N}$, for example, in spring the directly shined latitude is about at $A_1=12^\circ \text{ N}$ on the northern hemisphere. The air at the directly shined latitude is subjected to the solar radiation which forces the beat oscillation to run at the period $T_{beat}=1$ (year), where the air density varies as the sun-shine sways.

(2) Calm at the directly shined latitude with zero wind

Where the air constructively interferes with the solar radiation. This directly shined latitude A_1 is called as the **first constructive interference ridge**. Substituting zero wind into the above beat period formula, with $T_{beat}=1$ (year), we obtain the sun effect at the ridge:

$$v_{sun_effect_A_1} = 369.788 - \omega r \cos(A_1); \quad (units : m / s) \quad . \quad (16)$$

At other latitude A we should introduce inclination factor for the solar radiation, thus the global sun effect is given by

$$v_{sun_effect} = 369.788 \cos(A - A_1) - \omega r \cos(A) \quad . \quad (17)$$

(3) Wind formula

Calm at the ridge, while breeze winds nearby. Substituting the global sun effect into the above beat period formula, the wind under control of the beat T_{beat} nearby the ridge is given by

$$v_{wind} = \sqrt{\omega^2 r^2 - \frac{4\pi c^3}{\beta T_{beat}}} - \omega r \cos(A) - v_{sun_effect} \quad . \quad (18)$$

It is not easy to maintain the constructive interference condition. When the first constructive interference ridge is at latitude $A_1=12^\circ \text{N}$, the wind required for maintaining the beat period $T_{beat}=1$ (year) nearby is calculated by the above equation as shown in Fig.9(a) (blue line).

(4) The second ridge and third ridge

As the latitude A rises, the first ridge will be destroyed by destructive interference, but, the waves will again satisfy the constructive interference condition at next locations. According to calculation (see C source code for Fig.9), we find that at $A=39^\circ \text{N}$ location (second ridge) where beat $T_{beat}=0.5$ (years), and at $A=57^\circ \text{N}$ location (third ridge) where beat $T_{beat}=0.37$ (years) which is the shortest period that the earth can get within the arctic regions. The winds nearby the second ridge and third ridge are shown in Fig.9(a).

(5) Wind-curve over the northern hemisphere

The maximal wind appears at the midpoint of the first two ridges, about 48 (m/s). Linking all characteristic points in Fig.9(a) we obtain the predicted wind-curve over the northern hemisphere; this prediction agrees well with the experimental observations at an altitude of 10km (200hPa) [36], as shown in Fig.10. The zonal winds on the Jupiter has the same characteristics, as shown in Fig.8(b).

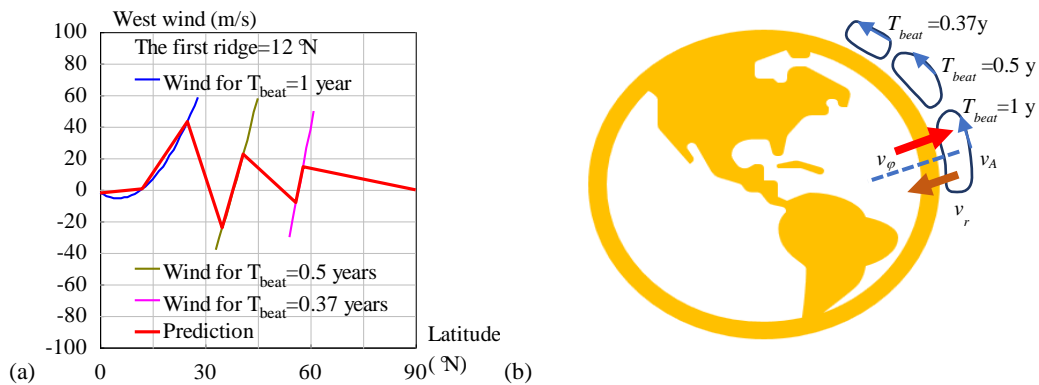


Fig.9 (a) Calculation of west winds in the northern hemisphere. (b) The atmospheric circulation in the northern hemisphere.

<Clet2020 Script>// C source code [26]

```

double beta,H,M,r,rc, rs, rot,v1,v2, Year,T,Lamda,V,a,b,w,Fmax,N[500],S[500],F[100]; int i, j, k, t, m, n, s, f,Type,x;
int main(){beta=1.377075e+14; H=SPEEDC*SPEEDC/SPEEDC/beta;
M=5.97237e24; rs=6.371e6; rot=2*PI/(24*3600); Year=24*3600*365.2422;
Type=1; x=10; if(Type>1) x=-30//v2=rs*rot; a=v2*v2-4*PI*H/Year; V=sqrt(a)-v2;
if(Type==1) SetAxis(X_AXIS,0,0,90,"Latitude#n( 'N);0;30;60;90;");
else SetAxis(X_AXIS,-90,-90,90,"Latitude#n( 'N);=90;-60;-30;0;30;60;90;");
SetAxis(Y_AXIS,-100,-100,100,"West wind (m/s):-100;-80;-60;-40;-20;0;20;40;60;80;100;");
DrawFrame(0x016a,Type,0xaffaf);//Polyline(2,"-90,0,90,0");
Check(15,k); if(k>24) k=24; if(k<-24) k=-24; //TextAt(100,10,"V=%f",V);
T=Year/2; Wind(); f=0; Findf(); t=N[m+m]; T=Year; Wind(); f=0; Findf();
SetPen(2,0xff); Polyline(n,N,x,70,"Wind for T#sdbeat#t=1 year"); if(Type>1) Polyline(s,S);
F[0]=N[0];F[1]=N[1]; F[2]=N[m+m]; F[3]=N[m+m+1]; t=(t+F[2])/2;//midst of two ridges
t=F[2]+m; Fmax=N[t+t+1]; //TextAt(100,20,"t=%d, Fmax=%f",t,Fmax);
f=Fmax; Findf(); F[4]=N[m+m]; F[5]=N[m+m+1];
T=Year/2; Wind(); f=Fmax/2; Findf(); t=m;f=Fmax/2; Findf();
SetPen(2,0x80ff00); Polyline(n,N,x,-50,"Wind for T#sdbeat#t=0.5 years"); if(Type>1) Polyline(s,S);
F[6]=N[t+t]; F[7]=N[t+t+1]; F[8]=N[m+m]; F[9]=N[m+m+1];
T=0.37*Year; Wind(); f=Fmax/4; Findf(); t=m;f=Fmax/4; Findf();
SetPen(2,0x9933fa); Polyline(n,N,x,-70,"Wind for T#sdbeat#t=0.37 years"); if(Type>1) Polyline(s,S);
F[10]=N[t+t]; F[11]=N[t+t+1]; F[12]=N[m+m]; F[13]=N[m+m+1]; F[14]=90; F[15]=0;
//Draw("ELLIPSE,0.2,XYX,10","15,20,25,35");TextHang(5,40,0,"a route");
SetPen(3,0xff0000); Polyline(8,F,x,-90,"Prediction"); TextHang(x,90,0,"The first ridge=%d 'N", k);
}
Wind(){n=0;s=0;
for(i=0;i<90;i+=1) { a=i*PI/180; b=(i-k)*PI/180; v1=rot*rs*cos(a); v2=rot*rs;
w=369.788*cos(b)-v2*cos(k*PI/180); a=v2*v2-4*PI*H/T; V=sqrt(a)-v1-w;
if(V>-40 && V<60) {N[n+n]=i; N[n+n+1]=V; n+=1;}}
for(i=0;i<90;i+=1) { a=i*PI/180; b=(-i-k)*PI/180; v1=rot*rs*cos(a); v2=rot*rs;
w=369.788*cos(b)-v2*cos(k*PI/180); a=v2*v2-4*PI*H/T; V=sqrt(a)-v1-w;
if(V>-40 && V<60) {S[s+s]=-i; S[s+s+1]=V; s+=1;}}
Findf(){a=1e10; for(i=0;i<n;i+=1) { b=N[i+i+1]-f;if(b<0) b=-b;if(b<a) {m=i;a=b;}}
} //if(k==12) ClipJob(APPEND,"i=%d,V=%f",i,V);
#v07=?>A#t

```

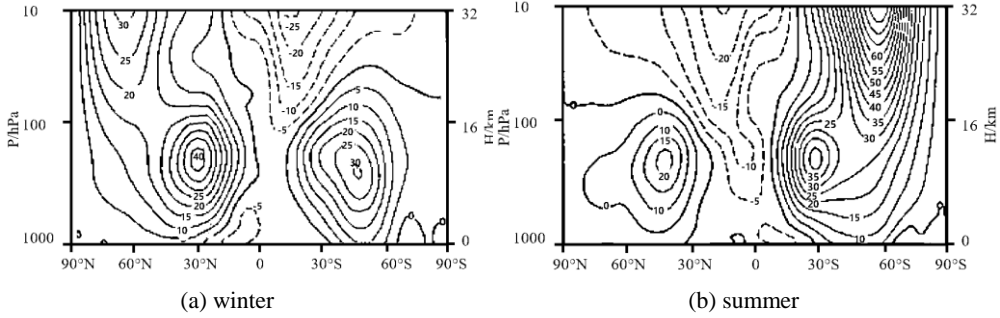


Fig.10 NCEP/NCAR data, mean west winds over 40 years (1958~1997) [36].

(6) Wind vector over the northern hemisphere

For further improvement of precision, the value of the wind should be resolved into three components in the spherical coordinates (r, A, φ) as

$$v_{wind}^2 = v_r^2 + v_A^2 + v_\varphi^2 \quad (19)$$

According to the energy equipartition theorem in thermodynamics, approximately we have their average estimation

$$\langle v_r^2 \rangle = \langle v_A^2 \rangle = \langle v_\varphi^2 \rangle = \frac{1}{3} v_{wind}^2 \quad (20)$$

Thus, the wind vectors over the northern hemisphere of the Earth are plotted in Fig.9(b), where the atmospheric circulation consists of three cells: Hadley cell, Ferrel cell, and arctic cell.

(7) Season clock

The beat $T_{beat}=1$ (year) works out **two seasons** (dry and rainy) in the tropic regions. The beat $T_{beat}=0.5$ (years) blows comfortable winds over Europe, Northern America and Northeastern Asia, and modulates out **four seasons** (spring, summer, autumn, winter), this beat is a well-known **season clock**. The arctic regions favor well-quantized beat $T_{beat}=1/3$ (years)

rather than the beat $T_{beat}=0.37$ (years), this situation gives rise to extra cold streams. The shortest beat $T_{beat}=0.37$ (years) has to adapt to the beat $T_{beat}=1/3$ (years) by emitting extra cold streams per 2.24 years to Europe, Northern America and Northeastern Asia, which is recognized as the **Rosby waves**.

(8) Easterlies at the equator

Since the relativistic matter wave of the air interferes with the relativistic matter wave of the earth shell, the easterlies at the equator have a magnitude of about 10 m/s in Fig.9(a). The trade winds or the easterlies are the permanent east-to-west **prevailing winds** that flow in the Earth's equatorial region. The trade winds blow mainly from the northeast in the Northern Hemisphere and the southeast in the Southern Hemisphere, strengthening during the winter and when the Arctic oscillation is in its warm phase. Trade winds have been used by captains of sailing ships to cross the world's oceans for centuries. The driving force of atmospheric circulation is the uneven distribution of solar heating across the earth, which is greatest near the equator and least at the poles. This air rises to the tropopause, about 10–15 kilometers above sea level, where the air is no longer buoyant [33].

7. Third example of gravity-clock: Human lifespan [30]

Human body consists of five parts: one head and four limbs, a heart pumps the blood to the whole body circularly. Consider a person sleeping in a bed with the head pointing to the North Pole, as shown in Fig.11(a), the five red lines from the heart represent its five artery tubes.

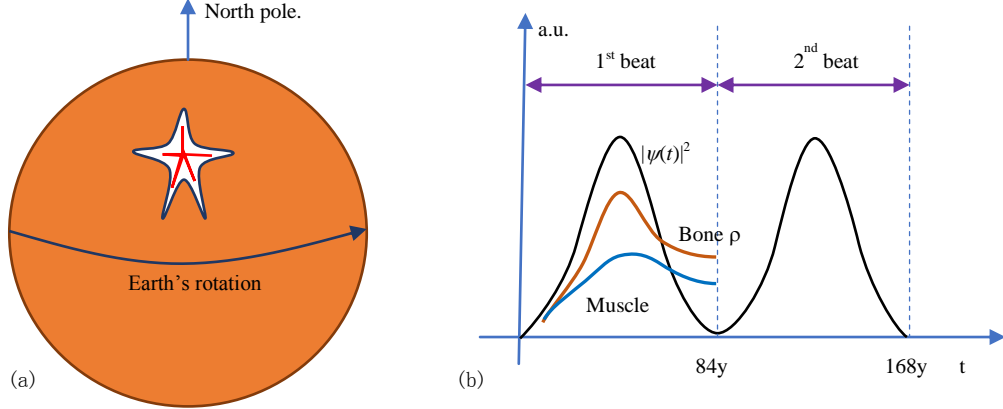


Fig.11 (a)A human sketch with the head pointing to the North Pole. (b) the biological gravity-clock.

Apparently, the arterial blood flows into the two arms with a speed, whose planetary-scale matter wave would interfere with the Earth's shell matter wave, producing a beat phenomenon:

$$|\psi|^2 = |\psi_{blood} + C\psi_{shell}|^2 = 1 + C^2 + 2C \cos\left[\frac{2\pi}{\lambda_{beat}} \int_L dl - \frac{2\pi}{T_{beat}} t\right] \quad (21)$$

$$\frac{2\pi}{T_{beat}} \approx \frac{\beta}{c^3} \left(\frac{v_{blood}^2}{2} - \frac{v_{shell}^2}{2} \right); \quad \frac{2\pi}{\lambda_{beat}} = \frac{\beta}{c^3} (v_{blood} - v_{shell}); \quad v_{shell} = \omega r$$

where C represents the coupling coefficient, ω is the Earth's angular speed, r the Earth radius. The shell's ψ_{shell} is with spherical symmetry because the earth's density $\rho(r)$ is approximately

spherical symmetry, so that this calculation carries out on the Earth's equator. The blood flow velocity varies with the location of blood vessels. The normal value of aortic valve orifice blood flow velocity in adults is 1.0-1.7m/s, and that in children is 1.2-1.8m/s. The flow velocity of carotid artery is less than 1.2m/s, the normal flow velocity of abdominal aorta is less than 1.8 m/s, and the normal flow velocity of inferior vena cava is 0.05-0.25m/s. Therefore, 1m/s is the order of magnitude of the blood velocities. Suppose the mean blood speed in human arms is 1m/s near the heart, in the Earth-orbital reference frame, the flowing blood suffers a beat with the period as the follows

$$v_{shell} = r\omega = 463.8m/s; \quad v_{blood} = v_{shell} \pm 1m/s$$

$$T_{beat} \approx \frac{4\pi c^3}{\beta(v_{blood}^2 - v_{shell}^2)} = \pm 84 \text{ (years)}; \quad \lambda_{beat} = 1.2e+12(m) \quad (22)$$

```
<Clet2020 Script>// [9]
double beta,H,M,r,rc, rs, rot,v1,v2, Year,T,Lamda,V,a,b,x,y,w;
int main(){beta=1.377075e+14; H=SPEEDC*SPEEDC*SPEEDC/beta;
M=5.97237e24; rs=6.378e6; rot=2*PI/(24*3600); Year=24*3600*365.2422;
v1=rot*rs;v2=v1+1; a=v2*v2-v1*v1; T=4*PI*H/a;
T/=Year; Lamda=2*PI*H/(v2-v1); b=Lamda/(2*PI*rs);
TextAt(100,20,"v1=%f, v2=%f, T=%f, L=%e, b=%e",v1,v2,T,Lamda,b);
T=2*PI*H/v1;T/=0.86;TextAt(100,50,"T=%e",T);
}#v07=?>A
```

In fact, the blood is pumped from the heart into both the eastern arm and western arm in Fig.11(a), producing a positive beat and a negative beat in the two arms with the same period 84 years, the two beats form an overall beat through the two arms. It is found that human mean lifespan is just confined within the single period duration, this beat period is recognized as the human biological **gravity-clock**. The beat wavelength λ is 30000 times the circumference of the earth, so its λ effects are hardly observed.

According to the explanation to ψ in the preceding section 2, the beat $|\psi|^2$ is proportional to the matter density.

$$|\psi|^2 \propto \rho \quad (23)$$

The $|\psi|^2$ oscillation of the beat in Fig.11(b) represents the variation of a human body density in his whole life confined within one beat period. The human bone density (red line) and muscle (blue line) in a human life vary as function of age, also responding to the $|\psi|^2$ oscillation, as shown in Fig.11(b). After astronauts entered the space station, the coupling between the astronauts and the earth's rotation decreased, and there was a significant decrease in bone density, indicating that the bone density of normal people on the earth's surface is strongly related to $|\psi|^2$.

8. Application to tropical cyclones

A tropical cyclone is a rapidly rotating storm system characterized by a low-pressure center, a closed low-level atmospheric circulation, strong winds, and a spiral arrangement of thunderstorms that produce heavy rain and squalls. Tropical cyclones on either side of the Equator generally have their origins in several tropical cyclone basins, as shown in Fig.12. The Northwest Pacific Ocean is the most active basin on the planet, accounting for one-third of all tropical cyclone activity. Warm sea surface temperatures are required for tropical cyclones to

form and strengthen. The commonly-accepted minimum temperature range for this to occur is 26–27 °C [37,38].

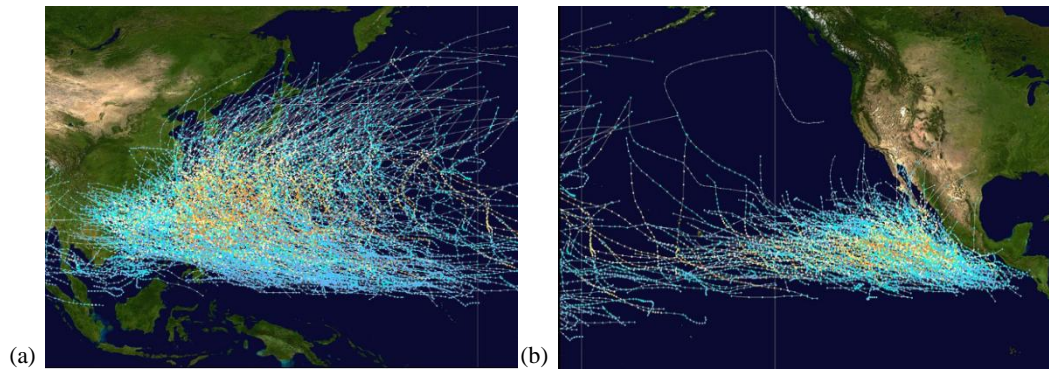


Fig.12 (a) Tracks of all tropical cyclones in the northwestern Pacific Ocean between 1980 and 2005.[39]. (b) Tracks of all tropical cyclones in the northern Pacific Ocean east of the International Date Line between 1980 and 2005.[39]

In every spring, the latitude $A=12^{\circ}\text{N}$ is called the **first constructive interference ridge**, is sandwiched between easterlies and westerlies, where the shear action of the winds will produce a lot of vortexes if the winds are disturbed by vapors at higher altitudes. The pregnancy of a tropical cyclone needs three steps, as shown in Fig.13(a).

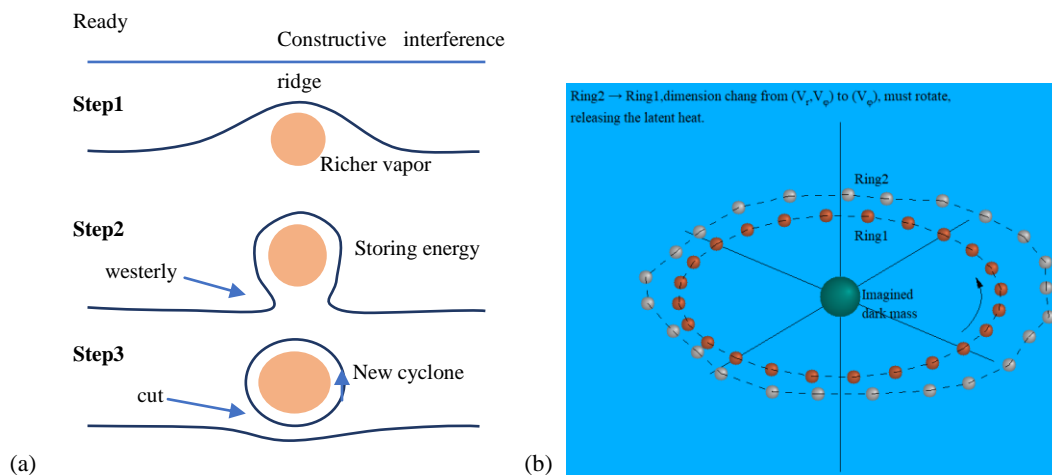


Fig.13 (a)Three steps for the pregnancy of a tropic cyclone in the northern hemisphere. (b) Dimension change on a molecular scale.

```
<Clet2020 Script>// C source code [26]
double r,x,y,z,v, a,b,c,dP[20],D[500]; int i,j,k ;
main(){ SetViewAngle("temp0,theta60,phi-40"); DrawFrame(FRAME_LINE,2,0xafff);
dP[0]=PEARL; dP[1]=0xefefef; dP[2]=1; dP[3]=XYZ;
dP[4]=10; dP[5]=10; dP[6]=0; dP[7]=50; dP[8]=30; dP[9]=30;
r=100; b=10; j=0;
for(i=0;i<360;i+=15) { a=i*PI/180; x=r*cos(a); y=r*sin(a); z=0;
x+=b*random(); y+=b*random();
D[j+j+j]=x; D[j+j+j+1]=y; D[j+j+j+2]=z; Plot(dP,D[j+j+j]); j+=1;}
Plot("POLYGON,1,@j,XYZ,10,",D);
r=80; b=6; dP[1]=0xf7f50; j=0;
for(i=0;i<360;i+=15) { a=i*PI/180; x=r*cos(a); y=r*sin(a); z=0;
D[j+j+j]=x; D[j+j+j+1]=y; D[j+j+j+2]=z; Plot(dP,D[j+j+j]); j+=1;}
Plot("POLYGON,1,@j,XYZ,10,",D);
TextHang(10,0,70,"Ring2#n#n#nRing1");
TextAt(100,200,"Ring2 → Ring1,dimension chang from (V#sdr#t,V#sdφ#t) to (V#sdφ#t), must rotate,#nreleasing the latent heat.");
D[0]=0; D[1]=0; D[2]=0; dP[1]=0x03a89e; dP[4]=30; dP[5]=30; Plot(dP,D);
TextHang(8,8,0,"Imagined #ndark mass"); r=70; j=0;
for(i=10;i<60;i+=5) { a=i*PI/180; x=r*cos(a); y=r*sin(a); z=0;
```

```

D[j+j]=x; D[j+j+1]=y; D[j+j+2]=z; j+=1;}
dP[0]=POLYLINE; dP[1]=3; dP[2]=j; dP[3]=XYZ; dP[4]=15; Plot(dP,D);
}#v07=?>A#t

```

Step1, during summer, the richer vapor at higher altitudes over the warm sea surface dramatically absorbs the solar radiation and releases the $v_{sun_effect} = -85(m/s)$ into the air at lower altitudes; consequently, the strengthened easterlies make a distortion to the first constructive interference ridge, as shown in Fig.13(a).

Step2, day by day, the distortion develops to an extent that it is going to separate from the mother-like first constructive interference ridge which is hit strongly by the westerlies, as shown in Fig.13(a).

Step3, finally, the distorted constructive interference ridge grows up to become an isolated baby ring which is recognized as a new tropical cyclone, counter-clockwise in the northern hemisphere, as shown in Fig.13(a), similar to Fig.8(b) there is a large vortex on the surface of Jupiter.

The pregnancy of tropical cyclones tends to develop at the latitude $A=12---23.5\text{ }^{\circ}\text{N}$, it is a relativistic quantum mechanical effect that cannot be solved by classical fluid mechanics. Actually, the solar radiation varies its mostly shined latitudes within the range of $A=23.5\text{ }^{\circ}\text{S} \sim 23.5\text{ }^{\circ}\text{N}$ due to the tilt of the earth axis concerning the earth orbital plan, therefore actual pregnancy latitudes of tropical cyclones occur among latitude angles $A=23.5\text{ }^{\circ}\text{S} \sim 23.5\text{ }^{\circ}\text{N}$, this result agrees well with the experimental records.

In Fig.9(a), there are the second, the third, ..., constructive interference ridges to bear the pregnancy of cyclones, hurricanes, typhoons, storms, tornados. Without these flexible constructive interference ridges, it is difficult for classical physics to say that some disturbances would somehow support the persistence of the vortexes.

For understanding the pregnancy process on a molecular scale, considering there are two molecular rings in Fig.13(b), typically the air molecules move on the Earth's surface in 2D motion. From ring2 to ring1, there is a dimension change for the molecules whose velocity changes from (v_r, v_ϕ) to (v_ϕ) , i.e. from 2D to 1D, losing the r component velocity. According to the energy equipartition theorem, every molecule would lose its kinetic energy as the latent heat released into the sky as

$$E_{latent} = \frac{2}{2} kT - \frac{1}{2} kT = \frac{1}{2} kT \quad (24)$$

At this moment, the molecules have to rotate about the cyclone's center. Losing an amount of the molecular kinetic energy will lead the ring1 to be in a stationary bound state, whose binding force and binding energy are given by

$$F_{centripetal} = -\frac{\Delta E}{\Delta r} = -\frac{N_{molecules} E_{latent}}{\Delta r} \quad (25)$$

$$E_{binding} = N_{molecules} E_{latent}$$

As you wish, you can say that at the cyclone's center there exists an **imagined dark mass** which contributes to this binding force by using the universal gravitational formalism.

When the constructive interference ring of a newly born cyclone forms a baby cyclone, its wavelength of the new air-vapor system will adapt to its ring size as

$$\frac{1}{hM_{cyclone}} \oint_L v_l dl = 2\pi n; \quad n = 1, 2, \dots \quad (26)$$

where the mass M represents the overall mass of the new baby cyclone, including the **imagined dark mass** which accounts for the latent heat released during its formation; the constant h of the baby cyclone is the **Planck-constant-like constant** determined by experimental observations.

The air molecules of the ring are under the control of their planetary-scale matter waves whose coherent length is so long that the waves have to overlap as

$$\psi(r) = 1 + e^{i\delta} + e^{i2\delta} + \dots + e^{i(N-1)\delta} = \frac{1 - \exp(iN\delta)}{1 - \exp(i\delta)} \quad (27)$$

$$\delta(r) = \frac{1}{hM_{cyclone}} \oint_L (v_l) dl$$

where N is the overlapping number which is determined by the coherent length of the relativistic matter wave, δ is the phase difference after one orbital motion. This formula can be used to calculate the distribution of the cyclone's density. In the preceding section 2, we have mentioned how to determine the N ; considering the tropic cyclone consisting of air-vapor, the overlapping number N of the air-vapor of the baby cyclone is simply estimated as $N=2$, the structure of tropical cyclones becomes easier to calculate, that is

$$\psi(r) = 1 + e^{i\delta} = 1 + \cos(\delta) + i \sin(\delta) \quad (28)$$

It follows that the full expression is given in 2D cylinder wave form by

$$\psi(r)_{interference} = \sqrt{\frac{r_0}{r}} \sin(\delta) e^{i(k_r r - \omega t)} = \sqrt{\frac{r_0}{r}} \sin\left(\frac{v 2\pi r}{hM}\right) e^{i(k_r r - \omega t)} \quad (29)$$

On altitude scale, a cyclone can be divided into two layers: the upper layer and the lower layer. In the lower layer at the first ring, the radius r_0 is proportional to the wavelength λ of the planetary-scale matter waves, the swirling wind speed approximately is inversely proportional to radius r , and the maximal speed is about 45 (m/s) according to the theoretical prediction of the maximal wind in Fig.9 (a) and the experimental observations [40] in Fig.14(a), then we have

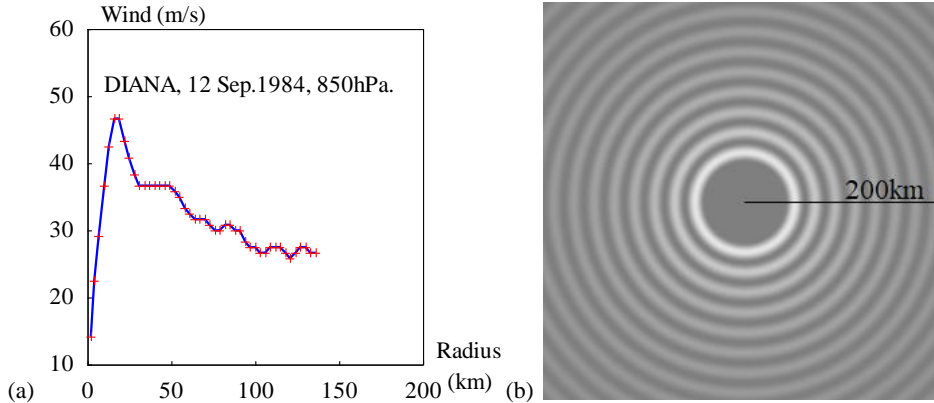


Fig.14 (a) Gradient wind as a function of the radius for the hurricane DIANA (12, Sep.1984) measured at 850hPa [40]. (b) The simulation of a cyclone, $|x| < 200\text{km}$.

<Clet2020 Script>// C source code [26]

```

int i,j,k,n; double x,y,nP[10];
int
D_Wind[92]={2,5,4,15,7,23,10,32,13,39,16,44,19,44,22,40,25,37,28,34,31,32,34,32,37,32,40,32,43,32,46,32,49,32,52,31,55,30,
58,28,61,27,64,26,67,26,70,26,73,25,76,24,79,24,82,25,85,25,88,24,91,24,94,22,97,21,100,21,103,20,106,20,109,21,112,21,115,
21,118,20,121,19,124,20,127,21,130,21,133,20,136,20,};
main(){SetAxis(X_AXIS,0.0,200,"Radius#n (km);0;50;100;150;200;");
SetAxis(Y_AXIS,0.0,60,"Wind (m/s); 10;20;30;40;50;60;");
DrawFrame(FRAME_BOX,1,0,affaf); j=46;
SetPen(2,0,ff); Polyline(j,D_Wind); SetPen(1,0,ff0000);
nP[0]=CROSS;nP[1]=0;nP[2]=j;nP[3]=XY;nP[4]=4;nP[5]=4;Plot(nP,D_Wind);
TextHang(10,50,0,"DIANA, 12 Sep.1984, 850hPa.");
}#v07=?>A#t

<Clet2020 Script>// C source code [26]
int i,j,k,nP[10]; double r_unit,Lamda,r,r0,r1,r2,v,v0,v1,w, a,b,delta, D[100];//1D array
main(){ w=150; r_unit=1e3;//km
r0=30*r_unit; r1=r0; Lamda=2*PI*r0; v0=15;v1=30;//m/s
DrawFrame(FRAME_NULL,1,0,affaf); nP[0]=SET; nP[1]=1; nP[2]=PX;
for(i=-w;i<w;i+=1) { for(j=-w;j<w;j+=1) { r2=i*i+j*j;r=sqrt(r2)*r_unit;
if(r>r0) {b=r0/r; v=v0+v1*b; } else {b=0; v=v0*b; }
delta=2*PI*v*2*PI*r/(v0*Lamda);
a=sin(delta); a*=a; a*=b;//2D cylinder wave attenuation
nP[3]=Colorize(1,0,fffff,a);D[0]=250+i;D[1]=250+j;D[2]=0;PixelJob(nP,D); } }
Draw("LINE,0,2,XY,10","0,0,100,0");TextHang(50,5,0,"200km");
}#v07=?>A#t

```

$$2\pi r_0 = \lambda; \quad v_r = \frac{hM}{2\pi} k_r \quad . \quad (30)$$

$$r > r_0 : \quad v_\phi = v_0 + v_1 \frac{r_0}{r}; \quad v_0 = 15(m/s); \quad v_1 = 30(m/s)$$

The simulation of the planetary-scale matter wave interference is carried out as shown in Fig.14(b), clearly showing the inner structure of a cyclone, compared well with the DIANA cyclone on 12 Sep. 1984 in situ observation measured by an aircraft [40] in Fig.14(a). Don't underestimate the profound role of the Planck-constant-like constant in cyclone structure; without it, all return to the classical fluid mechanics.

9. Why dimension change causes spin and uncertainty

Dimension is defined as the number of independent parameters in a mathematical space. In the field of physics, dimension is defined as the number of independent space-time coordinates. 0D is an infinitesimal point with no length. 1D is an infinite line, only length. 2D is a plane, which is composed of length and width. 3D is 2D plus height component, has volume.

In this section, we at first discuss how to measure dimension by a wave. In Fig.15(a), one puts earphones into ear, one gets a 1D wave in the ear tunnel.

$$1D: \quad y = A \sin(kr - \omega t) = \frac{A}{r^0} \sin(kr - \omega t) \quad . \quad (31)$$

where r is the distance between the wave emitter and the receiver. In Fig.15(b), if one touches a guitar spring, one gets a 2D cylinder wave.

$$2D: \quad y = \frac{A}{r^{1/2}} \sin(kr - \omega t) \quad . \quad (32)$$

In Fig.15(c), one turns on a music speaker, one gets a 3D spherical wave.

$$3D: \quad y = \frac{A}{r} \sin(kr - \omega t) \quad . \quad (33)$$

us use \mathbf{k} to denote the wave-vector, then the above 2D wave equation tells us

$$k_r^2 = k^2 - k_\phi^2; \quad k = \frac{2\pi}{\lambda}; \quad k_\phi = \pm \frac{1}{2r}. \quad (38)$$

The k_ϕ causes the 2D wave-vector \mathbf{k} to spin little by little as illustrated in Fig.16. The positive and negative k_ϕ corresponds to spin up and spin down respectively; as r goes to infinity, the spin effect vanishes off.

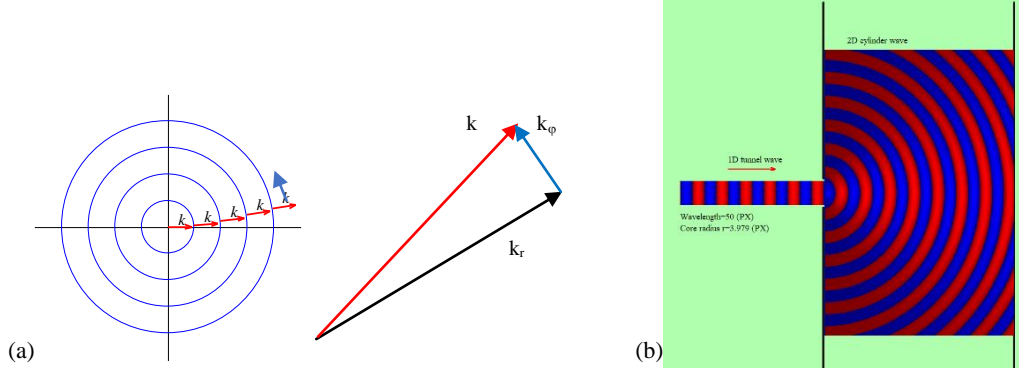


Fig.16 (a) 2D wave-vector \mathbf{k} spins little by little in the cylinder coordinates (r, ϕ) . (b) from 1D to 2D, the spin works to split the electron beam due to the double-value k_ϕ .

```
<Clet2020 Script>// C source code [26]
int i,j,k;double r,x,y,a,D[100];
int main(){DrawFrame(FRAME_LINE,1,0xafffaf);SetPen(1,0x0000ff);
for(i=0;i<90;i+=20){D[0]=-i;D[1]=-i;D[2]=i;D[3]=i;Draw("ELLIPSE,0,2,XY,0",D);}
for(i=0;i<90;i+=20){a=0.2*(i-i*200)*PI/180;r=i;D[0]=r*cos(a);D[1]=r*sin(a);
r+=18;D[2]=r*cos(a);D[3]=r*sin(a);SetPen(2,0xff0000);
Draw("ARROW,0,2,XY,8",D);TextHang(D[2]-10,D[3]+5,0,"#ifk");}
}#v07=?>A#
```

If the 2D wave is the de Broglie matter wave for a electron beam, in a cylinder coordinate (r, ϕ) , then the matter wave has a spin angular momentum J given by

$$k_r = \frac{p_r}{\hbar}; \quad k_\phi = \frac{p_\phi}{\hbar} = \frac{J}{r\hbar}; \quad J_\phi = \pm \frac{1}{2}\hbar. \quad (39)$$

According to the angular momentum formula in general physics, it is recognized that the particle total momentum p is a constant given by

$$\left(\frac{p}{\hbar}\right)^2 = \left(\frac{p_r}{\hbar}\right)^2 + \left(\frac{p_\phi}{\hbar}\right)^2 \quad k^2 = k_r^2 + k_\phi^2 = const. \quad (40)$$

Since the particle total wave vector k is a constant, the wave-vector k_r must vary as r changes. The wave-vector in the radial direction would change as the wave attenuates.

Applying the spin to tropic cyclones, the swirling speed including the spin speed and earth's self-rotation effect, etc., is simply given by

$$v = v_0 + v_1 \frac{r_0}{r}. \quad (41)$$

That is what was observed for tropic cyclones.

10. Conclusions

In analogy with the ultimate speed c , there is an ultimate acceleration β , nobody's acceleration can exceed this limit β , in the solar system, $\beta=2.956391e+10(m/s^2)$. Because this

ultimate acceleration is a large number, any effect related to β will become easy to test, including quantum gravity tests. In this paper, an approach is put forward to connect the ultimate acceleration with quantum theory, as an application, this approach is applied to tropic cyclone problems, the simulation is carried out, clearly showing the inner structure of a cyclone, which is very consistent with the famous DIANA cyclone on 12 September 1984 in situ observation measured by an aircraft.

References

- [1]C. Marletto, and V. Vedral, Gravitationally Induced Entanglement between Two Massive Particles is Sufficient Evidence of Quantum Effects in Gravity, *Phys. Rev. Lett.*, 119, 240402 (2017)
- [2]T. Guerreiro, Quantum effects in gravity waves, *Classical and Quantum Gravity*, 37 (2020) 155001 (13pp).
- [3]S. Carlip, D. Chiou, W. Ni, R. Woodard, Quantum Gravity: A Brief History of Ideas and Some Prospects, *International Journal of Modern Physics D*, V.24,14,2015,1530028. DOI:10.1142/S0218271815300281.
- [4]de Broglie, L., *CRAS*,175(1922):811-813, translated in 2012 by H. C. Shen in *Selected works of de Broglie*.
- [5]de Broglie, Waves and quanta, *Nature*, 112, 2815(1923): 540.
- [6]de Broglie, *Recherches sur la th orie des Quanta*, translated in 2004 by A. F. Kracklauer as *De Broglie, Louis, On the Theory of Quanta*. 1925.
- [7]NASA, <https://solarscience.msfc.nasa.gov/interior.shtml>.
- [8]NASA, <https://nssdc.gsfc.nasa.gov/planetary/factsheet/marsfact.html>.
- [9]B. Ryden *Introduction to Cosmology*, Cambridge University Press, 2019, 2nd edition.
- [10]D. Valencia, D. D. Sasselov,R. J. O'Connell, Radius and structure models of the first super-earth planet, *The Astrophysical Journal*, 656:545-551, 2007, February 10.
- [11]D. Valencia, D. D. Sasselov,R. J. O'Connell, Detailed models of super-earths: how well can we infer bulk properties? *The Astrophysical Journal*, 665:1413-1420, 2007 August 20.
- [12]T. Guillot, A. P. Showman, Evolution of "51Pegasus-like" planets, *Astronomy & Astrophysics*,2002, 385,156-165, DOI: 10.1051/0004-6361:20011624
- [13]T. Guillot, A. P. Showman, Atmospheric circulation and tides of "51Pegasus-like" planets, *Astronomy & Astrophysics*,2002, 385,166-180, DOI: 10.1051/0004-6361:20020101
- [14]L.N. Fletcher,Y.Kaspi,T. Guillot, A.P. Showman, How Well Do We Understand the Belt/Zone Circulation of Giant Planet Atmospheres? *Space Sci Rev*, 2020,216:30. <https://doi.org/10.1007/s11214-019-0631-9>
- [15]Y. Kaspi, E. Galanti, A.P. Showman, D. J. Stevenson, T. Guillot, L. Iess, S.J. Bolton, Comparison of the Deep Atmospheric Dynamics of Jupiter and Saturn in Light of the Juno and Cassini Gravity Measurements,*Space Sci Rev*, 2020, 216:84. <https://doi.org/10.1007/s11214-020-00705-7>
- [16]Orbital Debris Program Office, *HISTORY OF ON-ORBIT SATELLITE FRAGMENTATIONS*, National Aeronautics and Space Administration, 2018, 15 th Edition.
- [17]M. Mulrooney, The NASA Liquid Mirror Telescope, *Orbital Debris Quarterly News*, 2007, April,v11i2,
- [18]Orbital Debris Program Office, Chinese Anti-satellite Test Creates Most Severe Orbital Debris Cloud in History, *Orbital Debris Quarterly News*, 2007, April,v11i2,
- [19]A. MANIS, M. MATNEY, A. VAVRIN, D. GATES, J. SEAGO, P. ANZ-MEADOR, Comparison of the NASA ORDEM 3.1 and ESA MASTER-8 Models, *Orbital Debris Quarterly News*, 2021, Sept,v25i3.
- [20]D. Wright, Space debris, *Physics today*,2007,10,35-40.
- [21]TANG Zhi-mei, DING Zong-hua, DAI Lian-dong, WU Jian, XU Zheng-wen, "The Statistics Analysis of Space Debris in Beam Parking Model in 78   North Latitude Regions," *Space Debris Research*, 2017, 17,3, 1-7.
- [22]TANG Zhimei DING, Zonghua, YANG Song, DAI Liandong, XU Zhengwen, WU Jian the statistics analysis Of space debris in beam parking model based On the Arctic 500 MHz incoherent scattering radar, *CHINESE JOURNAL OF RADIO SCIENCE*, 2018, 25,5, 537-542
- [23]TANG Zhimei, DING, Zonghua, DAI Liandong, WU Jian, XU Zhengwen, Comparative analysis of space debris gaze detection based on the two incoherent scattering radars located at 69N and 78N, *Chin. J. Space Sci.*, 2018 38,1, 73-78. DOI:10.11728/cjss2018.01.073
- [24]DING Zong-hua, YANG Song, JIANG hai, DAI Lian-dong, TANG Zhi-mei, XU Zheng-wen, WU Jian, The Data Analysis of the Space Debris Observation by the Qujing Incoherent Scatter Radar, *Space Debris Research*, 2018, 18,1, 12-19.
- [25]YANG Song, DING Zonghua, Xu Zhengwe, WU Jian, Statistical analysis on the space posture, distribution, and scattering characteristic of debris by incoherent scattering radar in Qujing, *Chinese Journal of Radio science*, 2018 33,6 648-654, DOI:10.13443/j.cjors.2017112301
- [26]Clet Lab, Clet: a C compiler, <https://drive.google.com/file/d/1OjKqANcgZ-9V56rgcoMtOu9w4rP49sgN/view?usp=sharing>
- [27]Huaiyang Cui, Relativistic Matter Wave and Its Explanation to Superconductivity: Based on the Equality Principle, *Modern Physics*, 10,3(2020)35-52. <https://doi.org/10.12677/MP.2020.103005>
- [28]Huaiyang Cui, *Relativistic Matter Wave and Quantum Computer*, Amazon Kindle eBook, 2021.
- [29]Huaiyang Cui, (2023) Determination of Solar Radius and Earth's Radius by Relativistic Matter Wave, *Journal of Applied Mathematics and Physics*, 11:1, DOI: 10.4236/jamp.2023.111006
- [30]Huaiyang Cui, (2023) Biological Clock of Relativistic Matter Wave and Calculation of Human Mean Lifespan 84 Years, *Modern Physics (in Chinese)*, 2023, 13(2): 28-41. DOI: 10.12677/mp.2023.132005; Huaiyang Cui, (2023) Modelling of Human Lifespan -- Based on Quantum Gravity Theory with Ultimate Acceleration, *viXra:2302.0121*. <https://vixra.org/abs/2302.0121>
- [31]N.Cox. *Allen's Astrophysical Quantities*, Springer-Verlag, 2001, 4th ed.
- [32] S. E. Schneider, T. T. Arny, *Pathways to Astronomy*, McGraw-Hill Education, 2018, 5th ed.
- [33] https://en.wikipedia.org/wiki/El_Ni o%3C%3B%10%22%80%93Southern_Oscillation
- [34] https://en.wikipedia.org/wiki/Atmosphere_of_Earth
- [35] WANG Hui, WANG Aimei , LI Wenshan , LUO Jinxin , ZHANG Jianli, ZUO Changsheng, Changes in key indicators of coastal marine climate in China, *Marine Science Bulletin*, 2021, 23(1):17-34.
- [36] Liping Li et al, *Introduction to Atmospheric Circulation*, 2nd edition, Science Press, 2021,
- [37] https://en.wikipedia.org/wiki/Tropical_cyclone
- [38] https://en.wikipedia.org/wiki/Tropical_cyclone_basins
- [39] https://commons.wikimedia.org/wiki/File:Pacific_typhoon_tracks_1980-2005.jpg#/media/File:Pacific_typhoon_tracks_1980-2005.jpg. (a)
- [39] https://commons.wikimedia.org/wiki/File:Pacific_hurricane_tracks_1980-2005.jpg#/media/File:Pacific_hurricane_tracks_1980-2005.jpg. (b)
- [40] H.E. Willoughby, Gradient balance in tropical cyclones, *Journal of the Atmospheric Science*, 1990, Vol.47, 2, 263-274.